Li Kang,[1,2,3] Shilpa Mokshagundam,[1] Bradley Reuter,[1] Daniel S. Lark,[1] Claire C. Sneddon,[3] Chandani Hennayake,[3] Ashley S. Williams,[1] Deanna P. Bracy,[1,2] Freyja D. James,[1,2] Ambra Pozzi,[1,4,5] Roy Zent,[4,5] and David H. Wasserman[1,2]

Integrin-Linked Kinase in Muscle Is Necessary for the Development of Insulin Resistance in Diet-Induced Obese Mice

Diabetes 2016;65:1590–1600 | DOI: 10.2337/db15-1434

Diet-induced muscle insulin resistance is associated with expansion of extracellular matrix (ECM) components, such as collagens, and the expression of collagen-binding integrin, α2β1. Integrins transduce signals from ECM via their cytoplasmic domains, which bind to intracellular integrin-binding proteins. The integrin-linked kinase (ILK)-PINCH-parvin (IPP) complex interacts with the cytoplasmic domain of β-integrin subunits and is critical for integrin signaling. In this study we defined the role of ILK, a key component of the IPP complex, in diet-induced muscle insulin resistance. Wild-type (ILK$^{lox/lox}$) and muscle-specific ILK-deficient (ILK$^{lox/lox}$HSA*cre*) mice were fed chow or a high-fat (HF) diet for 16 weeks. Body weight was not different between ILK$^{lox/lox}$ and ILK$^{lox/lox}$HSA*cre* mice. However, HF-fed ILK$^{lox/lox}$HSA*cre* mice had improved muscle insulin sensitivity relative to HF-fed ILK$^{lox/lox}$ mice, as shown by increased rates of glucose infusion, glucose disappearance, and muscle glucose uptake during a hyperinsulinemic-euglycemic clamp. Improved muscle insulin action in the HF-fed ILK$^{lox/lox}$HSA*cre* mice was associated with increased insulin-stimulated phosphorylation of Akt and increased muscle capillarization. These results suggest that ILK expression in muscle is a critical component of diet-induced insulin resistance, which possibly acts by impairing insulin signaling and insulin perfusion through capillaries.

Insulin resistance is a commonly associated risk factor for many pathophysiological conditions, including diabetes, cardiovascular diseases, neurological changes, liver diseases, and sleep apnea (1,2). A defect in glucose utilization in the skeletal muscle is a major component of insulin resistance. The pathogenesis of muscle insulin resistance is not fully understood, and pharmacological interventions that reduce insulin resistance are limited and often lose efficacy over time (e.g., biguanides) or have adverse side effects (e.g., thiazolidinediones) (3). Our recent studies have suggested a novel role for extramyocellular factors in regulating muscle insulin action. Expansion of extracellular matrix (ECM) components, such as the collagens and the expression of the collagen-binding integrin α2β1, are associated with muscle insulin resistance induced by a high-fat (HF) diet (4). The ECM is in direct contact with the muscle capillaries. Defects in recruitment of muscle capillaries contribute to the development of muscle insulin resistance (5). Transduction of ECM signals through integrins requires interaction of the integrin cytoplasmic domains with cellular proteins. To investigate the link between ECM-integrin signaling and muscle insulin resistance, we studied a highly conserved central downstream component of the ECM-integrin signaling, integrin-linked kinase (ILK), and its role in muscle insulin resistance.

ILK, a pseudokinase with adaptor function, is a central component of the ILK-PINCH-parvin complex (IPP) (6). This complex binds to the cytoplasmic domain of β-integrin subunits. The IPP complex functions as an adaptor between integrins and the actin cytoskeleton, and therefore regulates multiple cellular functions, including cell

[1]Department of Molecular Physiology and Biophysics, Vanderbilt University, Nashville, TN
[2]Mouse Metabolic Phenotyping Center, Vanderbilt University, Nashville, TN
[3]Division of Molecular and Clinical Medicine, School of Medicine, University of Dundee, Dundee, U.K.
[4]Division of Nephrology, Department of Medicine, Vanderbilt University, Nashville, TN
[5]Department of Medicine, Veterans Affairs Hospital, Nashville, TN

Corresponding author: Li Kang, l.kang@dundee.ac.uk.

Received 16 October 2015 and accepted 23 March 2016.

This article contains Supplementary Data online at http://diabetes.diabetesjournals.org/lookup/suppl/doi:10.2337/db15-1434/-/DC1.

spreading, migration, proliferation, survival, and cell-cell adhesion (7,8). IPP also acts as a hub of the downstream of integrin signaling that regulates several other signaling pathways. The IPP complex associates with the receptor tyrosine kinase (RTK) pathways (e.g., insulin receptor pathway) through protein NCK2, which binds to PINCH (9). Considering the important role of RTK signaling in metabolism, we propose that ILK is fundamental to metabolic regulation. In the current study, we tested the hypothesis that the expansion of ECM collagen will amplify activation of integrin receptor signaling through ILK and regulate insulin signaling, thereby contributing to muscle insulin resistance. Muscle-specific ILK knockout mice were used to investigate the contribution of ILK signaling in chow-fed and HF-fed mice, a well-established model of insulin resistance (10). Our results reveal that integrin receptor signaling through ILK is critical to the pathogenesis of insulin resistance.

RESEARCH DESIGN AND METHODS

Mouse Models

All mice were housed in cages under conditions of controlled temperature and humidity with a 12-h light/dark cycle. Transgenic mice expressing *Cre* under a human α-skeletal actin (HSA or *ACTA1*) promoter (006149; The Jackson Laboratory) were crossed with floxed ILK mice ($ILK^{lox/lox}$) (11,12) to obtain the muscle-specific ILK-deficient mice ($ILK^{lox/lox}$HSA*cre*). All mice were on a C57BL/6J background and were fed a chow (5001; LabDiet) or HF diet (F3282; BioServ) starting at 3 weeks of age (at weaning), for 16 weeks, unless stated otherwise. All mice had ad libitum access to food and water. The calorie breakdown was 29% protein, 13% fat, and 58% carbohydrate for the chow diet, and 15% protein, 59% fat, and 26% carbohydrate for the HF diet. Noticeably, the HF diet is also a low protein, low carbohydrate diet compared with the chow diet. Male mice were used in the study because of their more robust insulin-resistant phenotype after HF feeding compared with female mice. In addition, female mice introduce a number of biological variables for which there are currently limited data, and as such, adequately interpreting results is difficult. Body composition was determined by a mq10 nuclear magnetic resonance analyzer (Brucker Optics). The Vanderbilt and Dundee Animal Care and Use Committees approved all animal procedures.

Hyperinsulinemic-Euglycemic Clamp

Catheters were implanted in a carotid artery and a jugular vein of mice for sampling and intravenous infusions 5 days before hyperinsulinemic-euglycemic clamp (validated insulin clamp [ICv]) (13). ICv (4 mU/kg/min) was performed on mice fasted for 5 h because they have ample glycogen stores and do not undergo the dramatic weight loss seen after an overnight fast (13). [3-^{3}H]glucose was infused to determine glucose flux rates (14). Blood glucose was clamped at ~150 mg/dL using a variable glucose infusion rate (GIR). Mice received washed erythrocytes from donors to prevent the drop in hematocrit that would otherwise occur. ICv was achieved by assessment of blood glucose every 10 min, with GIR adjusted as needed. Blood was taken at 80–120 min for the determination of [3-^{3}H]glucose. Clamp insulin was determined at t = 100 and 120 min. At 120 min, the clamp was sustained and a 13 μCi bolus of 2[^{14}C]deoxyglucose ([^{14}C]2DG) was administered. Blood was taken at 122–155 min for [^{14}C]2DG determination. Mice were anesthetized after the last sample, and tissues were excised.

ICv Plasma and Tissue Sample Processing and Glucose Flux Rate Determination

Plasma insulin was determined using the insulin ELISA kit (Millipore). Nonesterified fatty acid (NEFA) concentrations were measured by an enzymatic colorimetric assay (NEFA C kit; Wako Chemicals). Liver triglyceride was measured in ~100 mg frozen liver using the GPO triglyceride kit (T7532; Pointe Scientific). Plasma and tissue radioactivity of [3-^{3}H]glucose, [^{14}C]2DG, and [^{14}C]2DG-6-phosphate were determined as previously described (15). Glucose appearance (Ra), endogenous glucose appearance (EndoRa), and glucose disappearance (Rd) rates were determined using nonsteady-state equations (16). The glucose metabolic index (Rg) was calculated as described (17).

Immunohistochemistry

ILK, collagen IV (ColIV), laminin, CD31, and von Willebrand factor (vWF) were assessed by immunohistochemistry in paraffin-embedded gastrocnemius tissue sections (5 μm) using the following primary antibodies: anti-ILK (sc-20019, 1:150; Santa Cruz Biotechnology), anti-ColIV (ab6586, 1:100; Abcam), anti-laminin (Z0097, 1:3,000; DakoCytomation), anti-CD31 (550274, 1:200; BD Biosciences), and anti-vWF (A0082, 1:3,000; DakoCytomation). Slides were lightly counterstained with Mayer's hematoxylin. The EnVision+HRP/DAB System (DakoCytomation) was used to produce localized, visible staining. Images were captured using a QImaging MicroPublisher camera mounted on an Olympus upright microscope. Immunostaining was quantified by ImageJ or BIOQUANT Life Science 2009 software. ILK, ColIV, and laminin protein were measured by the integrated intensity of staining. Muscle vascularity was determined by counting CD31-positive structures and by measuring areas of vWF-positive structures. Average fiber diameter of gastrocnemius muscle was manually measured from laminin staining images. At least 15 fibers were measured per image and 6 images were measured per animal.

Immunoprecipitation and Immunoblotting

Gastrocnemius was homogenized as previously described (4). Protein (40 μg) was applied to SDS-PAGE gel. The following antibodies were used to detect respective proteins: ILK (sc-20019, 1:1,000; Santa Cruz Biotechnology), insulin receptor substrate 1 (IRS-1) (2382, 1:1000; Cell

Signaling Technology), phosphorylated (p)-Akt (Ser473, 9271, 1:1,000; Cell Signaling Technology), total Akt (9272, 1:1,000; Cell Signaling Technology), p-P38 (9211, 1:1,000; Cell Signaling Technology), total P38 (9212, 1:1,000; Cell Signaling Technology), p-extracellular signal–related kinase (ERK) 1/2 (4370, 1:2,000; Cell Signaling Technology), total ERK1/2 (4695, 1:1000; Cell Signaling Technology), p–*c*-Jun *N*-terminal kinase (JNK) (9251, 1:1,000; Cell Signaling Technology), total JNK (9252, 1:1,000; Cell Signaling Technology), and p-Tyr (PY99, sc-7020, 1:1,500; Santa Cruz Biotechnology). GAPDH (5174, 1:2,000; Cell Signaling Technology) was used as a loading control. For immunoprecipitation, 500 μg protein was precleared with 50 μL protein A/G PLUS-Agarose beads by incubation at 4°C for 1 h. The protein supernatant was incubated with the insulin receptor β (IR-β) antibody (3025, 1:50; Cell Signaling Technology) at 4°C overnight, and 20 μL protein A/G PLUS-Agarose was added and incubated. The mixture was centrifuged and the supernatant removed. The beads were washed four times, and centrifugation was repeated. Beads were resuspended and applied to SDS-PAGE gel. Immunoblots were probed with primary antibodies for PY99 (sc-7020, 1:1,500; Santa Cruz Biotechnology) and IR-β (4B8) (3025, 1:1,000; Cell Signaling Technology).

Food Intake and Wet Gastrocnemius Weight

Food intake and gastrocnemius muscle weight were measured in HF-fed mice after 27 weeks of HF feeding. Average food intake for light and dark cycle was measured by a Promethion system (Sable Systems International). Wet gastrocnemius muscle was collected and weighed from mice fasted for 5 h.

Statistical Analysis

Data are expressed as mean ± SEM. Statistical analyses were performed using the Student *t* test or two-way ANOVA, followed by Tukey post hoc tests, as appropriate. The significance level was $P < 0.05$.

RESULTS

To elucidate the role of ILK in muscle insulin resistance, muscle-specific ILK$^{lox/lox}$HSA*cre* and their wild-type littermate controls (ILK$^{lox/lox}$) were fed the chow or HF diet, which has been previously defined, to induce muscle insulin resistance (10). Immunohistochemical staining of ILK revealed that ILK was exclusively deleted from the muscle fibers of ILK$^{lox/lox}$HSA*cre* mice but remained in the other cell types, such as endothelial cells (Fig. 1*A*). HF diet feeding alone did not affect ILK expression in the muscle (Fig. 1*B*). Deletion of ILK in skeletal muscle fibers did not affect weight gain of mice on either diet (Fig. 2*A*). The percentage of fat and lean masses did not differ between ILK$^{lox/lox}$ and ILK$^{lox/lox}$HSA*cre* mice regardless of diet (Fig. 2*B* and *C*). Consistent with the unchanged percentage of lean mass, wet gastrocnemius muscle weight was similar between HF-fed ILK$^{lox/lox}$ and ILK$^{lox/lox}$HSA*cre* mice (Fig. 2*D*). Food intake was the same between the two groups of mice fed the HF diet (Fig. 2*E*).

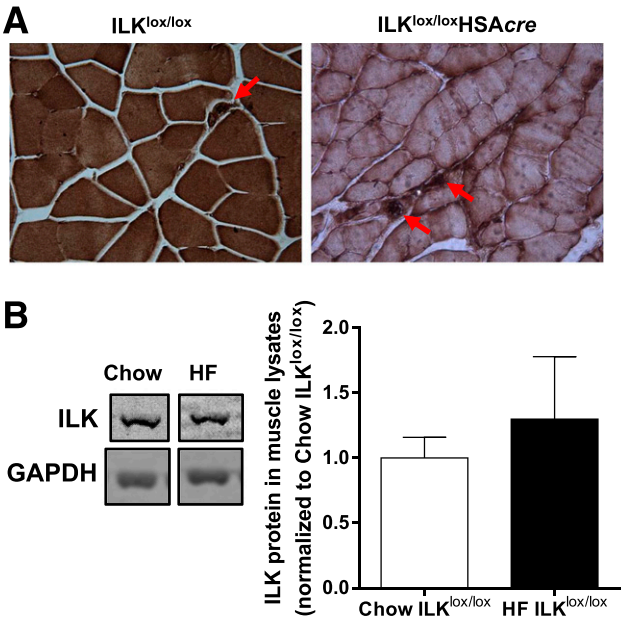

Figure 1—Protein expression of ILK in muscle. *A*: Immunohistochemical staining of ILK in paraffin-embedded gastrocnemius sections from chow-fed mice (n = 5). Representative images are presented at original magnification ×20, with the arrowheads indicating intact ILK expression in nonmyocytes. *B*: Western blotting of ILK in whole gastrocnemius muscle lysates from chow-fed and HF-fed ILK$^{lox/lox}$ mice (n = 3–4). Data are represented as mean ± SEM and are normalized to chow ILK$^{lox/lox}$.

To investigate the metabolic consequences of muscle-specific deletion of ILK, mice underwent ICv clamps. Basal arterial glucose (t = 0 min) was similar between chow-fed ILK$^{lox/lox}$ and ILK$^{lox/lox}$HSA*cre* mice but was significantly decreased in the HF-fed ILK$^{lox/lox}$HSA*cre* mice (Fig. 3*A* and *B*). ICv glucose during the steady state of the clamp (t = 80–120 min) was 150 mg/dL in both genotypes and in mice fed both diets (Fig. 3*A* and *B*). In chow-fed mice, ICv GIR was the same between ILK$^{lox/lox}$ and ILK$^{lox/lox}$HSA*cre* mice, indicating no difference in insulin sensitivity (Fig. 3*C*). Basal EndoRa and Rd were the same between chow-fed ILK$^{lox/lox}$ and ILK$^{lox/lox}$HSA*cre* mice (Fig. 3*E*). EndoRa was equivalently suppressed and Rd was equivalently increased during the ICv in both genotypes (Fig. 3*E*). In contrast, ICv GIR was markedly increased in the HF-fed ILK$^{lox/lox}$HSA*cre* mice compared with HF-fed ILK$^{lox/lox}$ mice, indicating an improved response to insulin (Fig. 3*D*). This increase in GIR in ILK$^{lox/lox}$HSA*cre* was due to an increase in clamp Rd (Fig. 3*F*). The inhibition of EndoRa during the ICv was unaffected by genotypes, emphasizing the muscle-specific effect on insulin action (Fig. 3*F*). Increased clamp Rd in HF-fed ILK$^{lox/lox}$HSA*cre* mice was attributed to increased glycolytic and to increased glucose storage rates, which were estimated by the rate of

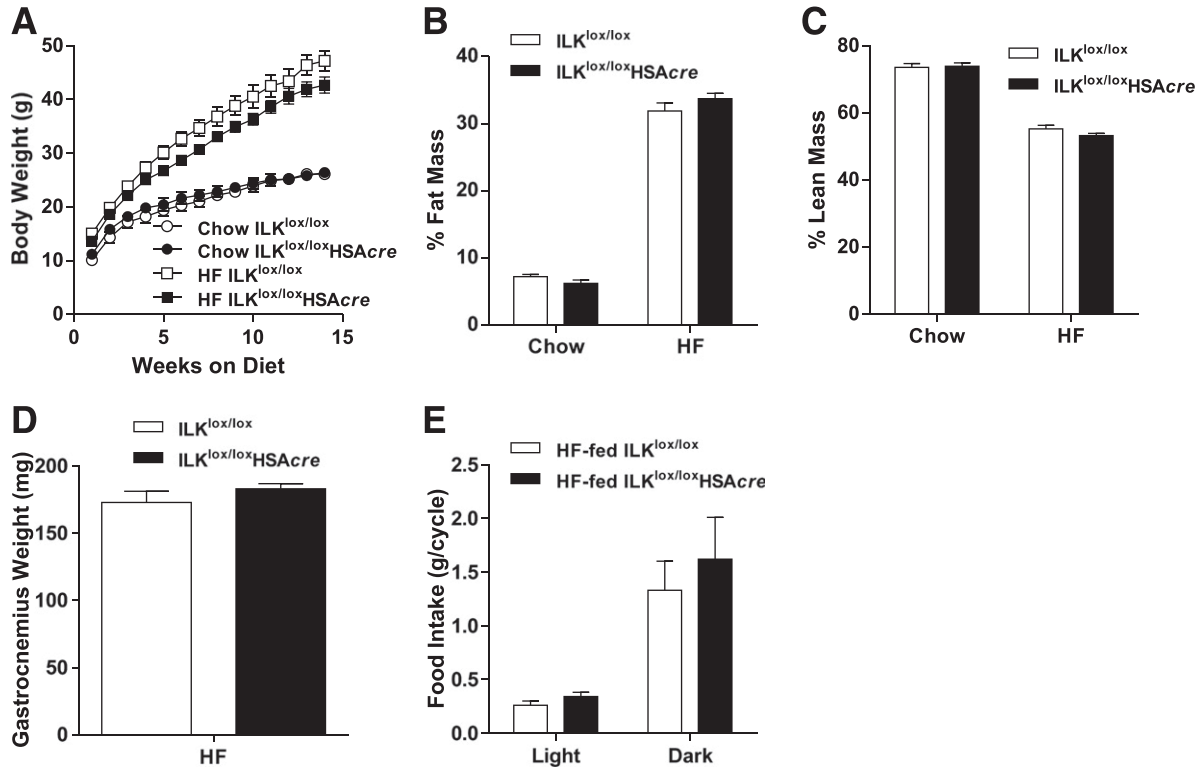

Figure 2—Body weight, body composition, gastrocnemius weight, and food intake of the muscle-specific ILK-deficient mice. *A*: Body weights of chow-fed and HF-fed ILK$^{lox/lox}$ and ILK$^{lox/lox}$HSA*cre* mice up to 14 weeks of diet starting at 3 weeks of age (n = 4–12). Percentages of fat (*B*) and lean masses (*C*) were determined in mice after 14 weeks of diet (n = 4–12). *D*: Gastrocnemius muscle was collected and weighed in mice fasted for 5 h after 27 weeks of the HF diet (n = 5). *E*: Food intake during the light and dark cycle was measured in mice after 27 weeks of the HF diet (n = 4). Data are represented as mean ± SEM.

plasma [^{3}H]H_2O accumulation during the ICv clamp (Supplementary Fig. 1).

Rg in muscles was decreased in HF-fed ILK$^{lox/lox}$ mice compared with chow-fed ILK$^{lox/lox}$ mice, indicative of HF diet–induced insulin resistance (Fig. 4*A*). Muscle Rg was unaffected by ILK deletion in chow-fed mice. Remarkably, the HF-induced muscle Rg impairment was absent in the HF-fed ILK$^{lox/lox}$HSA*cre* mice (Fig. 4*A*). Rg in adipose tissue was not different between ILK$^{lox/lox}$ and ILK$^{lox/lox}$HSA*cre* mice regardless of diet (Fig. 4*A*). Taken together, these data suggest that muscle-specific deletion of ILK in mice improved HF diet–induced insulin resistance specifically in muscle. This improvement of insulin resistance is independent of adiposity.

Basal plasma NEFA concentrations were not affected by genotype or diet (Fig. 4*B*). Despite the same plasma NEFA concentrations between chow-fed ILK$^{lox/lox}$ and ILK$^{lox/lox}$HSA*cre* mice during the ICv, ICv plasma NEFA was significantly lower in the HF-fed ILK$^{lox/lox}$HSA*cre* mice than in the HF-fed ILK$^{lox/lox}$ mice, indicative of an improved ability of insulin to inhibit lipolysis (Fig. 4*B*). Although basal arterial insulin was not affected by ILK deletion in the chow-fed mice, muscle-specific ILK deletion significantly lowered basal arterial insulin in the HF-fed mice, suggesting improved insulin sensitivity (Fig. 4*C*). It is worth noting that the basal arterial insulin concentration in HF-fed ILK$^{lox/lox}$HSA*cre* mice was still substantially higher than that in chow-fed mice. These data, together with a defect seen in glycogen storage in HF-fed ILK$^{lox/lox}$HSA*cre* mice compared with that in chow-fed mice (Supplementary Fig. 1), suggest that HF-fed ILK$^{lox/lox}$HSA*cre* mice were still insulin resistant despite the marked improvement in muscle Rg.

Insulin concentrations during the ICv were equivalent between genotypes (Fig. 4*C*). Even though insulin action in the liver, as assessed by EndoRa, was unaffected (Fig. 3*F*), liver triglyceride content was significantly decreased in the HF-fed ILK$^{lox/lox}$HSA*cre* mice compared with the HF-fed ILK$^{lox/lox}$ mice (Fig. 4*D*). This suggests that the muscle metabolic status can convey a signal to the liver that reduces triglyceride accumulation.

We also found similar changes in the status of adipose inflammation (Supplementary Fig. 2). Gene expression of total macrophage marker F4/80 was increased in ILK$^{lox/lox}$HSA*cre* mice compared with ILK$^{lox/lox}$ mice regardless of diet (Supplementary Fig. 2*A*). Gene expression of the proinflammatory marker tumor necrosis factor α was increased in ILK$^{lox/lox}$ mice by HF feeding, but interestingly this diet effect was absent in ILK$^{lox/lox}$HSA*cre* mice (Supplementary Fig. 2*B*). In contrast, gene expression

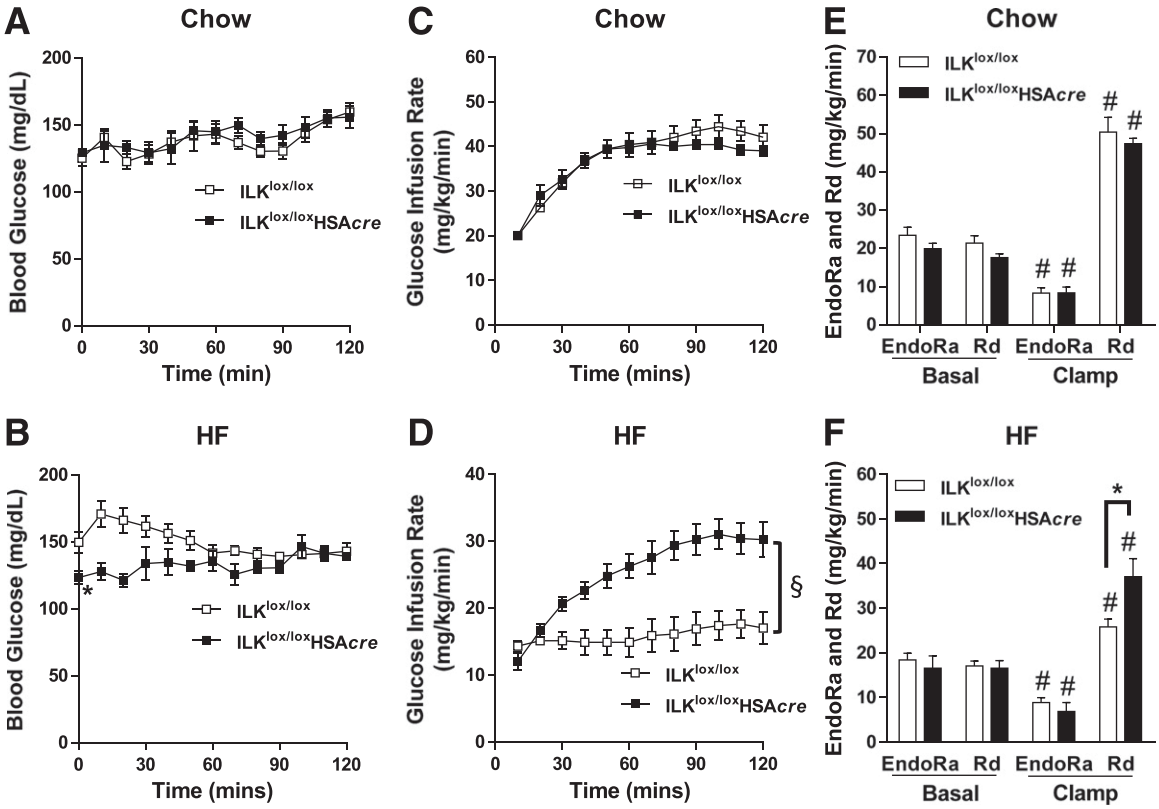

Figure 3—Insulin action as assessed by the hyperinsulinemic-euglycemic clamp (ICv). Mice underwent ICv experiments after 16 weeks of HF or chow-diet feeding at 19 weeks of age. *A* and *B*: Blood glucose during the ICv (n = 5–9). *C* and *D*: GIR during the ICv (n = 5–9). *E* and *F*: EndoRa and Rd rates were determined by [3-^{3}H]glucose (n = 5–9). All data are represented as mean ± SEM. *P < 0.05 HF-fed ILK$^{lox/lox}$ vs. HF-fed ILK$^{lox/lox}$HSA*cre*. #P < 0.05 basal vs. clamp with the same genotype. §P < 0.05 for the main genotype effect.

of the anti-inflammatory markers interleukin 10 and Arg-1 was increased in HF-fed ILK$^{lox/lox}$HSA*cre* mice compared with HF-fed ILK$^{lox/lox}$ mice (Supplementary Fig. 2*C*). These effects of muscle ILK deletion on liver and adipose tissue were associated with an increase in IL-6 mRNA levels in muscle of HF-fed ILK$^{lox/lox}$HSA*cre* mice compared with HF-fed ILK$^{lox/lox}$ mice (Supplementary Fig. 2*D*).

We further investigated the mechanisms by which HF-fed ILK$^{lox/lox}$HSA*cre* mice had improved muscle insulin resistance. Elevated ECM deposition has been associated with HF diet–induced muscle insulin resistance (4,18,19). We examined the ECM collagen and laminin content in the muscle. Consistent with previous findings (4), muscle ColIV deposition was increased by twofold with HF feeding in ILK$^{lox/lox}$ mice, but muscle laminin deposition was not affected (Fig. 5*A* and *B*). Neither ColIV nor laminin was affected by ILK deletion. Moreover, the average fiber diameter of gastrocnemius muscle was not changed by genotype or the HF diet (Fig. 5*C*). Interestingly, improved muscle insulin resistance in HF-fed ILK$^{lox/lox}$HSA*cre* mice was associated with increased CD31 staining in muscle of HF-fed ILK$^{lox/lox}$HSA*cre* mice compared with HF-fed ILK$^{lox/lox}$ mice, indicating increased CD31-positive capillarization (Fig. 5*D* and *E*). There was no change in vWF staining, indicating that larger vessels were unaffected (Fig. 5*D* and *E*).

We next investigated insulin signaling in the muscle. Although improved muscle insulin resistance in HF-fed ILK$^{lox/lox}$HSA*cre* mice was not associated with increased phosphorylation of insulin receptor (Fig. 6*A* and *B*) or IRS-1 (Fig. 6*C* and *D*), improved muscle insulin action was associated with increased phosphorylated and total Akt/protein kinase B (Fig. 6*C* and *E*). This effect is specific to insulin-stimulated conditions because phosphorylated and total Akt/protein kinase B was not increased in the basal 5 h-fasted muscles (Fig. 6*F* and *G*).

Mitogen-activated protein kinases (MAPKs) have been shown to negatively regulate endothelial cell survival, proliferation, and differentiation (20). We investigated whether the increased muscle capillarization in the HF-fed ILK$^{lox/lox}$HSA*cre* mice were associated with altered MAPKs pathway. Although HF diet feeding caused an increase in the p-P38–to–P38 and p-JNK–to–JNK ratios, this diet effect was absent in the HF-fed ILK$^{lox/lox}$HSA*cre* mice (Fig. 7*A*–*D*). Moreover, the p-ERK–to–ERK ratio was decreased in the HF-fed ILK$^{lox/lox}$HSA*cre* compared with HF-fed ILK$^{lox/lox}$ mice (Fig. 7*E* and *F*). These results are consistent with the prior assertion that capillarization may be upregulated by a decrease in MAPK activation (20).

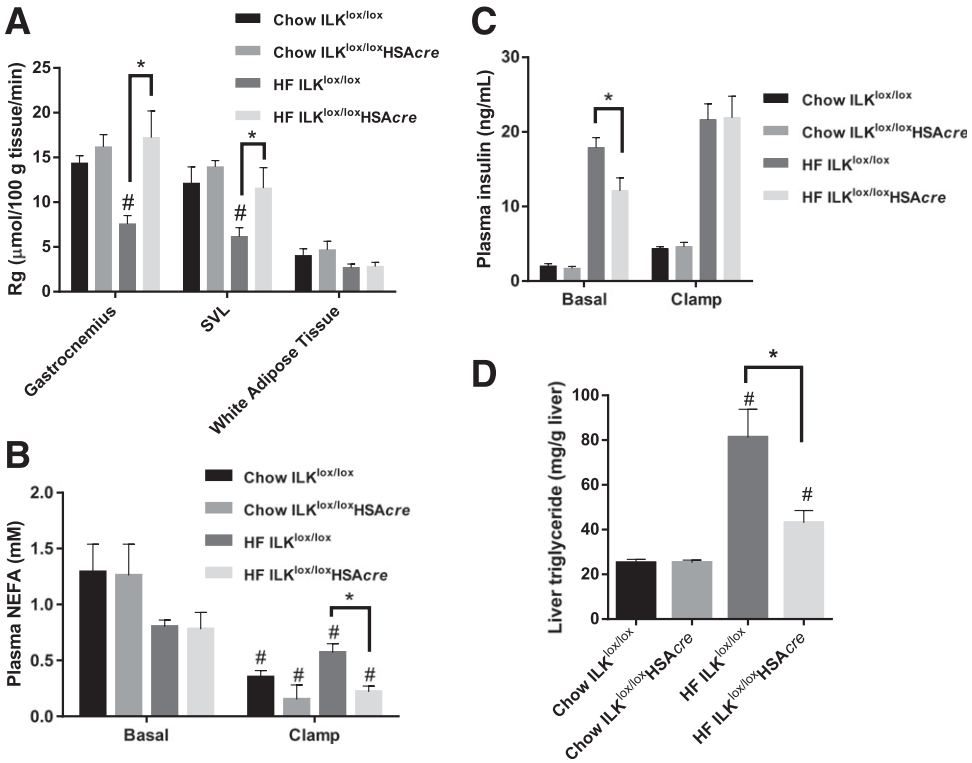

Figure 4—Muscle glucose uptake, circulating insulin, plasma NEFA, and liver triglyceride. *A*: Rg was determined by 2-[^{14}C]deoxyglucose (n = 5–9). SVL, superficial vastus lateralis. *B*: Plasma NEFA was determined at basal (−15 and −5 min) and during the steady state of the ICv (80 and 120 min) (n = 5–9). *C*: Plasma insulin concentration was measured at basal (−15 and −5 min) and during the steady state of the ICv (100 and 120 min) (n = 5–9). *D*: Liver triglyceride was determined in liver samples collected at the end of the ICv (n = 5–9). Data are represented as mean ± SEM. #P < 0.05 chow vs. HF with the same genotype. *P < 0.05.

DISCUSSION

ECM expansion and the interaction of protein constituents with the cell surface receptor integrin α2β1 were recently found to contribute to the pathogenesis of HF diet–induced muscle insulin resistance (4,18,19). There appear to be α-subunit–specific effects of integrin-ligand binding (21), because integrin α1β1 does not appear to contribute to diet-induced muscle insulin resistance (4,22). The ILK pseudokinase is a central component of the IPP complex that binds to the cytoplasmic domains of both integrin α1β1 and α2β1, and therefore its expression may be a better reflection of the integrated integrin response. Here we show that although muscle-specific deletion of ILK has no effect in lean, chow-fed mice, it improves HF diet–induced muscle insulin resistance. The improvement in insulin-stimulated glucose fluxes is specific to muscle because the ability of insulin to inhibit hepatic glucose production and to stimulate glucose uptake in adipose tissue are not affected. We further discovered that improved muscle insulin resistance in the ILK-deficient mice is associated with increased phosphorylation of Akt and increased muscle capillarization. These findings show that ILK is central to insulin resistance associated with HF feeding. An extension of these findings is that ILK inhibition is of potential therapeutic use in the treatment of diabetes and other insulin resistance–associated metabolic disorders.

We establish a working model in the current study by which insulin signaling and integrin signaling interact at the level of Akt (Fig. 8). Although ILK is a pseudokinase, it contains a catalytically inactive remnant of an active kinase that uses its substrate recognition motif to interact with other proteins that have well-conserved motifs required for eukaryotic protein kinase activity (23). Our results show that muscle-specific deletion of ILK increases phosphorylation of Akt at Ser 473 in HF-fed mice and that this effect is specific to insulin stimulation because basal Akt phosphorylation was not affected in these mice. The precise steps in the process of how ILK regulates phosphorylation of Akt during the stimulation of insulin are uncertain, but studies of ILK in cell adhesion and survival provide a basis for linkage. Rictor directly interacts with ILK and regulates Akt phosphorylation promoting cancer cell survival (24). Moreover, it is widely proposed that ILK associates with the RTK pathways (e.g., insulin receptor pathway) through protein NCK2, which binds to PINCH, one of the components of the IPP complex (9). The other possibility is that ILK controls Akt activity by regulating its subcellular localization because ILK-binding partners, α- and β-parvins,

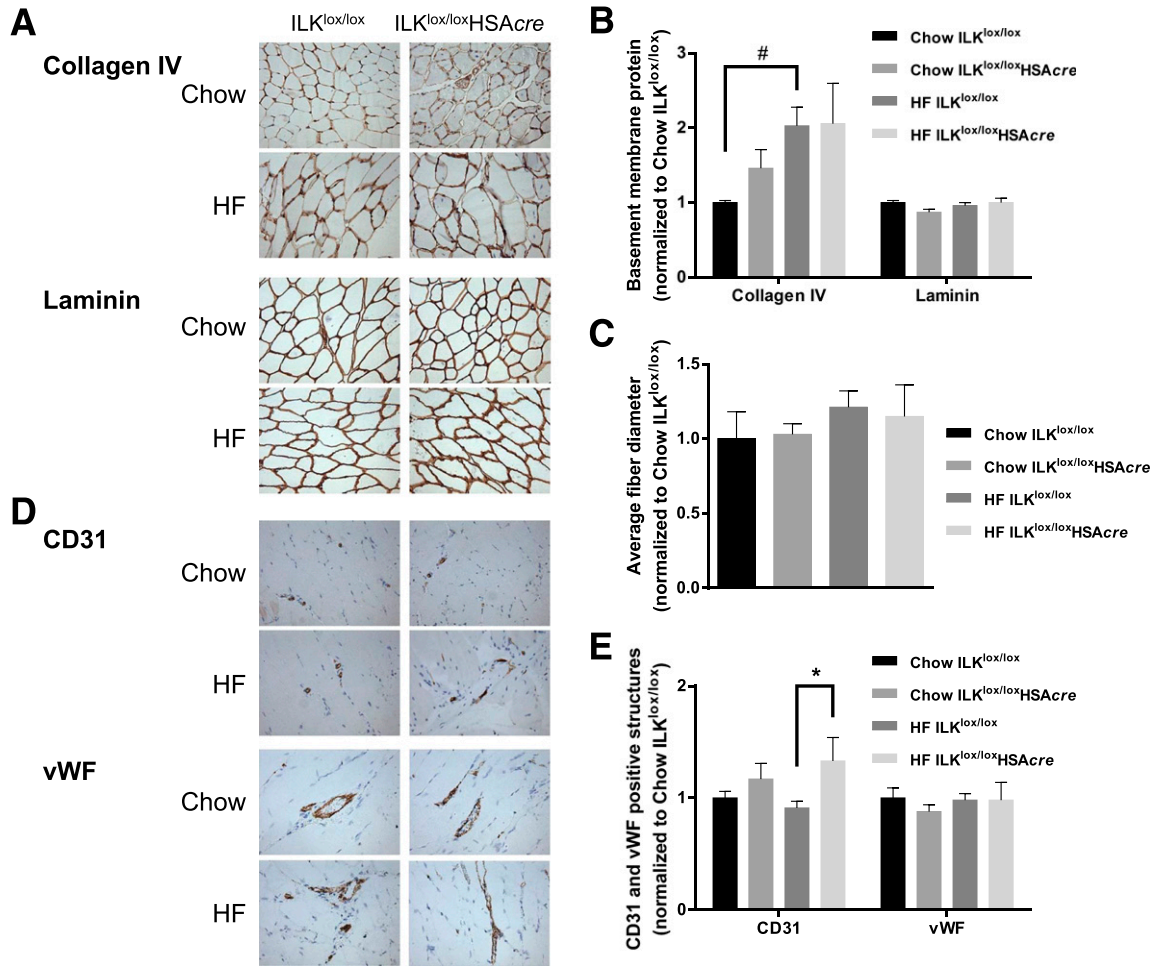

Figure 5—Muscle ECM deposition, fiber diameter, and vascular markers of the muscle-specific ILK-deficient mice. *A*: Immunohistochemical detection of ColIV and laminin in paraffin-embedded gastrocnemius sections (n = 5–9). Representative images are presented at original magnification ×20. *B*: Values of integrated intensity of staining for ColIV and laminin are presented as mean ± SEM, and data are normalized to chow ILK$^{lox/lox}$. #$P < 0.05$. *C*: Average fiber diameter was manually measured from laminin staining images (n = 5–9). *D*: Immunohistochemical staining of CD31 and vWF in paraffin-embedded gastrocnemius sections (n = 5–9). Representative images are presented at original magnification ×20. *E*: Values represent mean ± SEM of numbers of CD31-positive structures or of areas occupied by vWF-positive structures. Data are normalized to chow ILK$^{lox/lox}$. *$P < 0.05$.

induce the recruitment of Akt to the plasma membrane (25,26). It is noteworthy that most of studies in ILK have focused on signaling involved in cell spreading, adhesion, migration, and survival; therefore, the ILK-mediated signaling in metabolic regulation could be significantly different.

Reduction in blood flow to the muscle correlates with insulin resistance, and the number of capillaries that perfuse the muscle is positively related to peripheral insulin action (27). In the current study, we found that improvement of muscle insulin resistance in HF-fed obese mice by muscle-specific ILK deletion is associated with increased expression in muscle of vascular/endothelial marker CD31. This finding is consistent with a previous study that shows that genetic integrin α2β1 deletion–improved muscle insulin resistance is associated with increased muscle capillaries (4). In contrast, exacerbated insulin resistance in HF-fed mice deficient in matrix metalloproteinase 9, where muscle collagen deposition is increased, is associated with decreased muscle capillaries (19). Activation of MAPK pathways negatively regulates endothelial cell survival, proliferation, and differentiation (20). We found that increased muscle capillarization in the HF-fed ILK-deficient mice is associated with decreased phosphorylation of several MAPKs, including P38, ERK1/2, and JNK. The regulation of ILK in the MAPK pathways is thought to be through Ras suppression protein 1, which binds to ILK via Pinch-1 (28). Taken together, these results indicate that ILK expression in muscle may stimulate activation of various MAPKs pathways, which in turn inhibit capillary proliferation and endothelial function (Fig. 8). Inhibited phosphorylation of Akt and inhibited capillary proliferation induced by muscle ILK expression during insulin stimulation are likely mechanisms that both

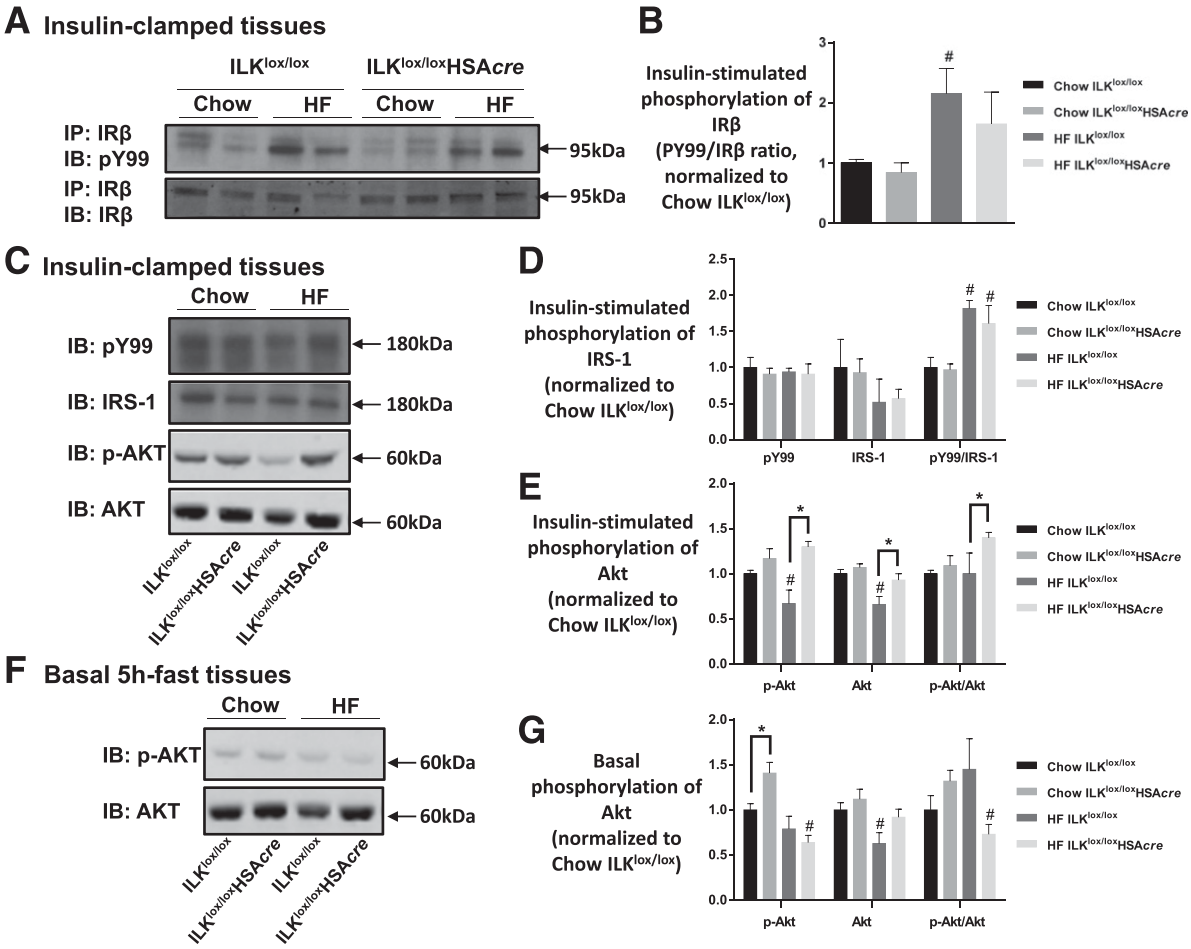

Figure 6—Insulin signaling in the muscle. Muscle homogenates were prepared from gastrocnemius collected from mice after the hyperinsulinemic-euglycemic clamp *(A–E)* or from mice after a basal 5-h fast *(F* and *G)*. *A*: IR-β was immunoprecipitated (IP), followed by immunoblotting (IB) of PY99 and IR-β. Representative bands are presented (n = 4–6). *B*: Quantitative data for panel *A*. *C*: p-IRS-1 was determined by immunoblotting of PY99 at 180 kDa. Total IRS-1, p-Akt, and total Akt were measured by Western blotting. Representative bands are presented (n = 4–6). *D*: Quantitative data for the Western blotting of PY99 at 180 kDa and total IRS-1 from panel *C*. *E*: Quantitative data for the Western blotting of p-Akt and total Akt from panel *C*. Data are normalized to chow $ILK^{lox/lox}$. *F*: Western blotting of p-Akt and total Akt in basal 5-h–fasted gastrocnemius tissues (n = 4). *G*: Quantitative data for panel *F*. Data are represented as mean ± SEM. #$P < 0.05$ chow vs. HF with the same genotype. *$P < 0.05$.

contribute to the development of insulin resistance in the presence of the HF diet (Fig. 8).

The effect of muscle-specific deletion of ILK on overall total blood flow in muscle is unknown. That ILK deletion has a major effect on muscle blood flow is unlikely because the expression of vWF, a vascular marker for bigger vessels, was not changed in the ILK-deficient mice (Fig. 5*D* and *E*). However, the increase in CD31 suggests that capillarization is increased. We hypothesize that improved muscle capillarization leads to greater exchange of insulin and other hormones from blood to muscle. Improved insulin access to muscle could contribute to improved insulin action in the HF-fed ILK-deficient mice.

Considerable evidence in the literature suggests that HF diet–induced insulin resistance in skeletal muscle is associated with a remodeling of actin cytoskeleton, which is worth noting (29). ILK, as a central component of the IPP complex that links integrins to actin cytoskeleton, is essential for actin cytoskeleton organization and morphology (30). Deletion of ILK in muscle possibly improves HF diet–induced insulin resistance through effects on reorganization of the actin cytoskeleton. Moreover, deletion of ILK in muscle may cause an alteration in muscle fiber type during HF feeding. This seems unlikely, however, because Gheyara et al. (31) previously showed that ILK deletion does not change muscle fiber type proportions or distribution in the quadriceps of chow-fed mice. Nevertheless, we cannot rule out that a switch in muscle fiber type to a more oxidative profile could occur during HF feeding and contribute to improved muscle insulin resistance in mice lacking muscle ILK.

Muscle-specific deletion of ILK has been shown to cause a progressive muscular dystrophy (31). This phenomenon is associated with disrupted focal adhesion proteins,

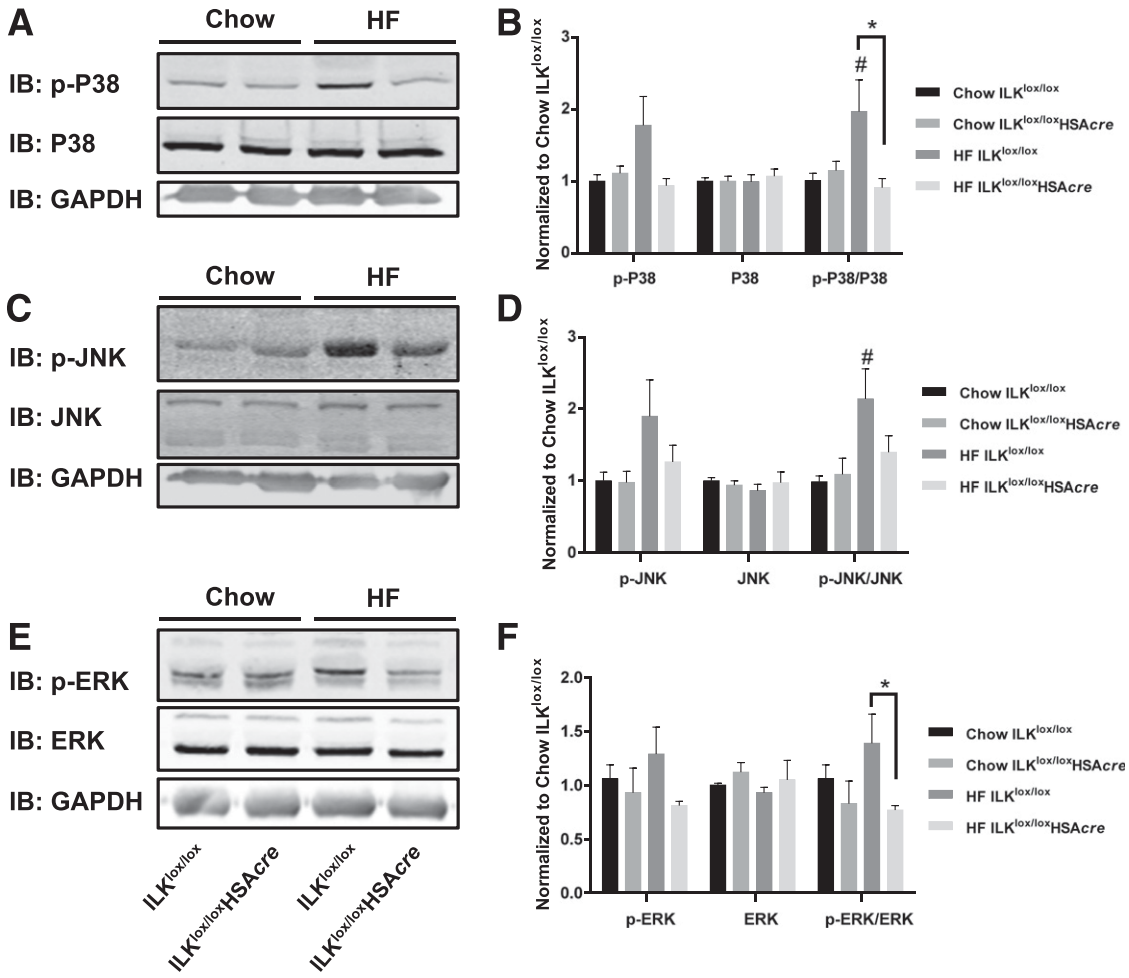

Figure 7—P38, JNK, and ERK MAPKs in the muscle. Western immunoblotting (IB) of p-P38 and total P38 (*A*), p-JNK and total JNK (*C*), and p-ERK and total ERK *(E)* in gastrocnemius homogenates isolated from mice after the hyperinsulinemic-euglycemic clamp. Representative bands are presented (n = 4–6). *B*, *D*, and *F*: Quantitative data for the Western blotting. Data are represented as mean ± SEM and are normalized to chow $ILK^{lox/lox}$. #$P < 0.05$ chow vs. HF with the same genotype. *$P < 0.05$.

including vinculin, paxillin, focal adhesion kinase, dystrophin, and the integrin α7β1 specifically at the myofascial junction regions. Gheyara et al. (31) reported that the muscle damage was limited to the myofascial junction regions in young ILK-mutant mice. Our current study focused at the muscle fiber level and was able to show, using immunohistochemistry, that ILK was specifically deleted from the muscle fibers. We showed that muscle collagens and laminin expression were not affected by ILK deletion. Importantly, we showed that total body weight and the percentage of fat and percentage of lean mass of chow-fed and HF-fed mice were unchanged by ILK deletion. These results suggest that although ILK deletion may have aging-related structure and focal adhesion phenotypes in the myofascial junction areas, it retains a robust insulin-stimulatory response.

The development of pharmacological inhibition of ILK by small-molecule inhibitors has primarily focused on inhibiting its kinase activity (32,33). Because ILK is a scaffold protein rather than a kinase, none of these inhibitors are specific to ILK. We therefore believe that the development of pharmacological inhibition of ILK that targets its binding motifs is under high demand in future studies. Our studies show that ILK deletion has a remarkable effect on improving insulin sensitivity. Thus, these studies further implicate the importance of inhibition of ILK in the setting of diabetes and associated metabolic disorders.

In conclusion, our results suggest that muscle-specific deletion of ILK markedly improves muscle insulin sensitivity in HF-fed insulin-resistant mice via increased phosphorylation of Akt in addition to increased muscle capillarization. The increased capillarization is associated with decreased phosphorylation of MAPKs. These studies are the first linking ECM-integrin signaling to muscle insulin resistance via ILK and provide a mechanistic framework for the importance of ECM-integrin-ILK in metabolic regulation. The results open the door to the

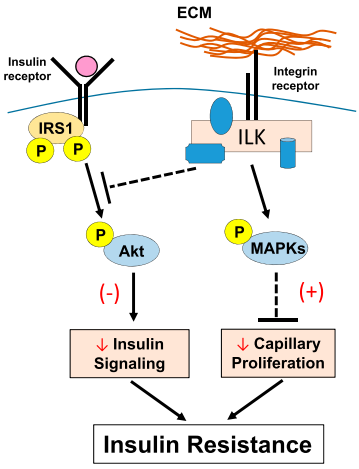

Figure 8—Proposed mechanisms by which ECM-integrin-ILK signaling regulates muscle insulin resistance in HF-fed mice. It is proposed that ILK will inhibit phosphorylation of Akt in the presence of insulin stimulation. ILK also stimulates the phosphorylation and activation of JNK, P38, and ERK1/2 MAPKs, which in turn inhibits capillary proliferation and therefore endothelial function in the muscle. Decreased phosphorylation of Akt and inhibited capillary proliferation both contribute to muscle insulin resistance during the HF feeding. (–) Represents diminished effects. (+) Represents potentiated effects.

development of inhibitors of ILK signaling in the treatment of insulin resistance and its related metabolic disorders.

Acknowledgments. The floxed ILK mice were generously provided by Professor Reinhard Fässler of Max Planck Institute of Biochemistry in Martinsried, Germany.

Funding. L.K. is supported by European Commission Marie Curie International Incoming Fellowship (FP7-PEOPLE-2013-IIF) and TENOVUS Scotland. This work was supported by National Institute of Diabetes and Digestive and Kidney Diseases grants DK-059637 (Vanderbilt Mouse Metabolic Phenotyping Center), T32-DK-070061 (D.S.L.), RO1-DK-095761 (A.P.), RO1-DK-083187 (R.Z.), RO1-DK-075594 (R.Z.), RO1-DK-066921 (R.Z.), and DK-054902 (D.H.W.), by National Institutes of Health grant RO1-CA-162433 (A.P.), and was partly supported by VA Merit Review 1I01BX002025 (A.P.) and 1I01BX002196 (R.Z.).

Duality of Interest. No potential conflicts of interest relevant to this article were reported.

Author Contributions. L.K. contributed to the experimental design, researched data, contributed to discussion, and wrote the manuscript. S.M., B.R., D.S.L., C.C.S., C.H., D.P.B., and F.D.J. researched data and reviewed and edited the manuscript. A.S.W. contributed to discussion and reviewed and edited the manuscript. A.P., R.Z., and D.H.W. contributed to the experimental design, reviewed data, contributed to discussion, and reviewed and edited the manuscript. All authors approved the final version of this manuscript. The authors received no editorial assistance. L.K. is the guarantor of this work and, as such, had full access to all the data in the study and takes responsibility for the integrity of the data and the accuracy of the data analysis.

Prior Presentation. This study was presented at the 74th Scientific Sessions of the American Diabetes Association, San Francisco, CA, 13–17 June 2014.

References

1. Dineley KT, Jahrling JB, Denner L. Insulin resistance in Alzheimer's disease. Neurobiol Dis 2014;72:92–103
2. Reutrakul S, Van Cauter E. Interactions between sleep, circadian function, and glucose metabolism: implications for risk and severity of diabetes. Ann N Y Acad Sci 2014;1311:151–173
3. Inzucchi SE, Bergenstal RM, Buse JB, et al. Management of hyperglycaemia in type 2 diabetes: a patient-centered approach. Position statement of the American Diabetes Association (ADA) and the European Association for the Study of Diabetes (EASD). Diabetologia 2012;55:1577–1596
4. Kang L, Ayala JE, Lee-Young RS, et al. Diet-induced muscle insulin resistance is associated with extracellular matrix remodeling and interaction with integrin alpha2beta1 in mice. Diabetes 2011;60:416–426
5. Bonner JS, Lantier L, Hocking KM, et al. Relaxin treatment reverses insulin resistance in mice fed a high-fat diet. Diabetes 2013;62:3251–3260
6. Legate KR, Montañez E, Kudlacek O, Fässler R. ILK, PINCH and parvin: the tIPP of integrin signalling. Nat Rev Mol Cell Biol 2006;7:20–31
7. Hannigan G, Troussard AA, Dedhar S. Integrin-linked kinase: a cancer therapeutic target unique among its ILK. Nat Rev Cancer 2005;5:51–63
8. Elad N, Volberg T, Patla I, et al. The role of integrin-linked kinase in the molecular architecture of focal adhesions. J Cell Sci 2013;126:4099–4107
9. McDonald PC, Fielding AB, Dedhar S. Integrin-linked kinase–essential roles in physiology and cancer biology. J Cell Sci 2008;121:3121–3132
10. Surwit RS, Kuhn CM, Cochrane C, McCubbin JA, Feinglos MN. Diet-induced type II diabetes in C57BL/6J mice. Diabetes 1988;37:1163–1167
11. Grashoff C, Aszódi A, Sakai T, Hunziker EB, Fässler R. Integrin-linked kinase regulates chondrocyte shape and proliferation. EMBO Rep 2003;4:432–438
12. Sakai T, Li S, Docheva D, et al. Integrin-linked kinase (ILK) is required for polarizing the epiblast, cell adhesion, and controlling actin accumulation. Genes Dev 2003;17:926–940
13. Ayala JE, Bracy DP, McGuinness OP, Wasserman DH. Considerations in the design of hyperinsulinemic-euglycemic clamps in the conscious mouse. Diabetes 2006;55:390–397
14. Berglund ED, Li CY, Poffenberger G, et al. Glucose metabolism in vivo in four commonly used inbred mouse strains. Diabetes 2008;57:1790–1799
15. Ayala JE, Bracy DP, Julien BM, Rottman JN, Fueger PT, Wasserman DH. Chronic treatment with sildenafil improves energy balance and insulin action in high fat-fed conscious mice. Diabetes 2007;56:1025–1033
16. Steele R, Wall JS, De Bodo RC, Altszuler N. Measurement of size and turnover rate of body glucose pool by the isotope dilution method. Am J Physiol 1956;187:15–24
17. Kraegen EW, James DE, Jenkins AB, Chisholm DJ. Dose-response curves for in vivo insulin sensitivity in individual tissues in rats. Am J Physiol 1985;248:E353–E362
18. Kang L, Lantier L, Kennedy A, et al. Hyaluronan accumulates with high-fat feeding and contributes to insulin resistance. Diabetes 2013;62:1888–1896
19. Kang L, Mayes WH, James FD, Bracy DP, Wasserman DH. Matrix metalloproteinase 9 opposes diet-induced muscle insulin resistance in mice. Diabetologia 2014;57:603–613
20. Matsumoto T, Turesson I, Book M, Gerwins P, Claesson-Welsh L. p38 MAP kinase negatively regulates endothelial cell survival, proliferation, and differentiation in FGF-2-stimulated angiogenesis. J Cell Biol 2002;156:149–160
21. McCall-Culbreath KD, Zutter MM. Collagen receptor integrins: rising to the challenge. Curr Drug Targets 2008;9:139–149
22. Williams AS, Kang L, Zheng J, et al. Integrin α1-null mice exhibit improved fatty liver when fed a high fat diet despite severe hepatic insulin resistance. J Biol Chem 2015;290:6546–6557
23. Wickström SA, Lange A, Montanez E, Fässler R. The ILK/PINCH/parvin complex: the kinase is dead, long live the pseudokinase! EMBO J 2010;29:281–291
24. McDonald PC, Oloumi A, Mills J, et al. Rictor and integrin-linked kinase interact and regulate Akt phosphorylation and cancer cell survival. Cancer Res 2008;68:1618–1624
25. Fukuda T, Guo L, Shi X, Wu C. CH-ILKBP regulates cell survival by facilitating the membrane translocation of protein kinase B/Akt. J Cell Biol 2003;160:1001–1008
26. Kimura M, Murakami T, Kizaka-Kondoh S, et al. Functional molecular imaging of ILK-mediated Akt/PKB signaling cascades and the associated role of beta-parvin. J Cell Sci 2010;123:747–755

27. Solomon TP, Haus JM, Li Y, Kirwan JP. Progressive hyperglycemia across the glucose tolerance continuum in older obese adults is related to skeletal muscle capillarization and nitric oxide bioavailability. J Clin Endocrinol Metab 2011;96:1377–1384
28. Kadrmas JL, Smith MA, Clark KA, et al. The integrin effector PINCH regulates JNK activity and epithelial migration in concert with Ras suppressor 1. J Cell Biol 2004;167:1019–1024
29. Habegger KM, Penque BA, Sealls W, et al. Fat-induced membrane cholesterol accrual provokes cortical filamentous actin destabilisation and glucose transport dysfunction in skeletal muscle. Diabetologia 2012;55:457–467
30. Hao YC, Yu LP, Li Q, et al. Effects of integrin-linked kinase on human corpus cavernosum smooth muscle cell cytoskeletal organisation. Andrologia 2013;45: 78–85
31. Gheyara AL, Vallejo-Illarramendi A, Zang K, et al. Deletion of integrin-linked kinase from skeletal muscles of mice resembles muscular dystrophy due to alpha 7 beta 1-integrin deficiency. Am J Pathol 2007;171:1966–1977
32. Yau CY, Wheeler JJ, Sutton KL, Hedley DW. Inhibition of integrin-linked kinase by a selective small molecule inhibitor, QLT0254, inhibits the PI3K/PKB/mTOR, Stat3, and FKHR pathways and tumor growth, and enhances gemcitabine-induced apoptosis in human orthotopic primary pancreatic cancer xenografts. Cancer Res 2005;65:1497–1504
33. Kalra J, Warburton C, Fang K, et al. QLT0267, a small molecule inhibitor targeting integrin-linked kinase (ILK), and docetaxel can combine to produce synergistic interactions linked to enhanced cytotoxicity, reductions in P-AKT levels, altered F-actin architecture and improved treatment outcomes in an orthotopic breast cancer model. Breast Cancer Res 2009;11:R25